

# Cutting and Shield Gases Pressure Effects on Plasma Cutting Quality

## Experimental observation of kerfs obtained with varying current and shield and cutting pressures

BY S. CHABERT, J. J. GONZALEZ, AND P. FRETON

### Abstract

In this paper, the effects of the shield gas on cut quality in plasma arc cutting were quantified experimentally. Measurements were performed on plasma arc cutting kerfs (PACs) cut through a 4 mm (1/8 in.) S355 steel plates with a Gys Neocut105 cutter equipped with a *Toparc* AT-125 torch. This system uses compressed air as both cutting and shield gas. Separate circuits for shielding air and cutting air were used. This way, the influences of the shield air and the cutting air could be studied independently. A full 3-factor, 3-level Taguchi design was followed. The studied factors are the cutting air pressure, the shield air pressure, and the arc current. The measured responses are the removed steel surface and the right and left bevel angles. As expected, the current proved to have the greatest influence on the kerf surface. The cutting air pressure significantly influenced the kerfs' shapes while the shield air flow rate proved less important yet sensitive. Some negative bevel angles at high plasma, high cutting, and high shield air pressures have also been observed.

### Keywords

- Plasma Arc Cutting
- Bevel Angles
- Taguchi
- Kerf Measurement
- Shield Gas

### Introduction

#### Background

Plasma arc cutting, used to cut metals, offers an interesting compromise between speed, accuracy, and cost for intermediate thicknesses as compared to laser and oxycutting (Refs. 1–2). It uses a transferred arc and the plate to be cut is used as the anode. The process uses cutting gas and shield gas (both compressed air in our study). A hot plasma melts the metal and blows it away, thus creating a kerf. Kerfs display various qualities.

#### Literature Review

There are numerical studies about the kerf quality problem. For example, Hendricks (Ref. 3) has numerically found that increasing current or reducing torch speed increases plate maximum temperature, kerf size, and heat-affected zone (HAZ) surrounding a kerf and in which the heat modifies the metal crystal structure). Also, Nemchinsky and Severance (Refs. 4–5) propose a numerical approach to determine top and bottom kerf widths and bevel angles depending on torch speed: increasing speed leads to narrower top kerf width and greater bevel angles, which means even narrower bottom kerf widths. The interaction between factors, i.e., mass flow and current is complex and leads to non-monotonic results regarding kerf width (Ref. 6).

Several authors (Refs. 7–10) have also been interested in the experimental characterization of cutting quality. Mostly, the MRR (Material Removal Rate, the volume of metal removed during the cut process during a given time), bevel angles, rugosity, and HAZ are studied through arc current, torch speed, and torch height variations. High currents lead to high MRR and HAZ. Concerning the other parameters, the results vary according to the operating parameters and can adopt non-monotonic behaviors.

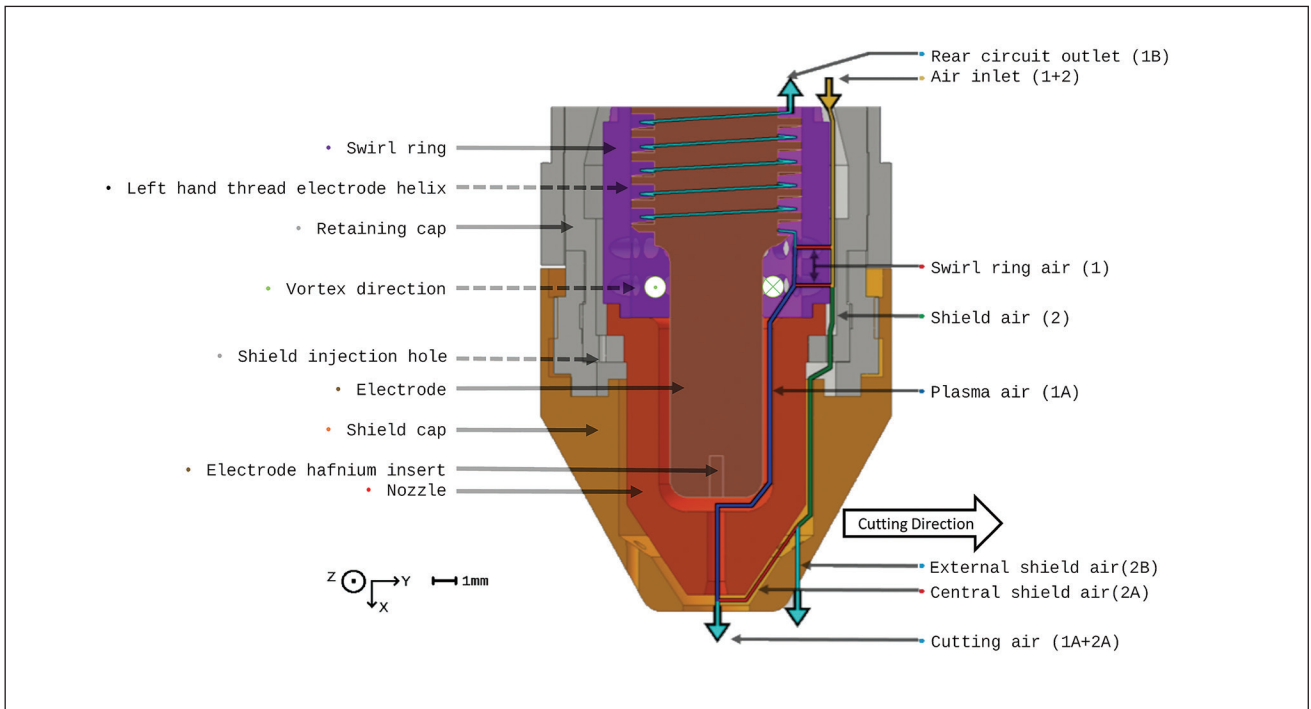


Fig. 1 – Torch diagram showing AT-125 head parts and effluxes circuits.

Illi et al. (Ref. 11) and Nemchinsky et al. (Ref. 12) have also shown that torch speed, torch height, gas pressure, and nature were highly impacting factors over cut quality. Notably, dross formation is strongly dependent on torch speed. There is a window of speeds allowing no-dross cuts. Low-speed dross occurs when the cut speed subsides that window and may be removed easily, whereas high-speed dross is hard to break. In this study, the samples displayed some low-speed dross, but they were cleaned effortlessly. Dross is not considered in this paper.

Shield gas is used in most modern plasma cutting systems to prevent molten metal projections from damaging the torch and helps cool the nozzle down. It can also form a protective atmosphere in multi-gas cutting systems (which is not the case in this paper). However, its effects on the kerf geometry are not well documented.

## Purpose

Even if several papers (Refs. 7–11) deal with operating parameters' impact on cut quality, this work is original in that it considers the plasma air pressure along with the shield air pressure and shows their influences on kerf shape.

The following section introduces the studied torch geometry and the way it works. Then the prototype used in this study to control the plasma and the shield air pressures separately is presented. Afterward, the design of the experiments is described. It defines the scope of the study regarding the factor's range. Then the equipment used during the experiment as well as the cutting protocol are described. The measurement protocol is also detailed. Next, the calculations through which measurements were processed are outlined.

Finally, the results are discussed, particularly the effects of shield air pressure on kerf's shape.

## Experimental Procedure and Setup

### Base Torch

The plasma cutter used is a Gys Neocut105 which can generate an arc up to 105 A. It was equipped with a *Toparc* AT-125 torch (which is designed to operate up to 125 A). This system uses pressurized air as cutting and shielding gases. Figure 1 shows the original torch head lower parts along the air effluxes circuits and their names (in bold and between brackets). The hose that feeds air and current to the torch and the torch head's upper parts are not represented. A settable pressure regulator inside the generator body feeds the air to the torch. The swirl ring air (1) is the sum of the cutting air (1A) and rear cooling air (1B). It is granted a swirl component (Ref. 13) and is injected all around the electrode by the swirl ring. It also separates the electrode from the nozzle when fed, allowing lift arc ignition. The electrode is equipped with an erosion-resistant hafnium insert. The electrode feeds current to the plasma. It gets constricted by the nozzle and blown onto the cut material. The rear circuit (1B) helps cool the electrode down. The retaining cap holds the components together and channels the effluxes. There are ten shield injection holes inside the retaining cap that feed air to the shield air circuit (2). This circuit is subdivided into two sections: the external shield air (2B) that helps protect the torch from molten metal projections, and the central shield air (2A) that greatly helps cool down the nozzle. It is

**Table 1 – Pressures and Corresponding Flow Rates at I = 105 A**

Original Setup at 105 A	
$Q_1 = 152 \text{ NL/min}$ at $P_1 = 5 \text{ bar}$	$Q_2 = 80 \text{ NL/min}$ at $P_1 = 5 \text{ bar}$
Prototype Setup at 105 A	
$Q_1 = 152 \text{ NL/min}$ at $P_1 = 4.6 \text{ bar}$	$Q_2 = 80 \text{ NL/min}$ at $P_2 = 0.28 \text{ bar}$
$Q_1 = 100 \text{ NL/min}$ at $P_1 = 3 \text{ bar}$	$Q_2 = 0 \text{ NL/min}$ at $P_2 = 0 \text{ bar}$
$Q_1 = 200 \text{ NL/min}$ at $P_1 = 6 \text{ bar}$	$Q_2 = 160 \text{ NL/min}$ at $P_2 = 0.97 \text{ bar}$

**Table 2 – Domain of Study in the Scope of Taguchi’s Method**

Factor	$P_1$ (bar)	$P_2$ (bar)	I (A)
Level 1	3	0	45
Level 2	4.6	0.28	75
Level 3	6	0.97	105

the shield cap that channels the 2A and 2B effluxes along with shielding the inner parts of the torch.

### Shield Cap Prototype

The aim here is to study the influence of the air pressures on the cut quality. Mostly, it is about determining whether the shield gas also has an influence or not. However, the original system, as seen in Figs. 1 and 2A, is not designed to have the inputs to these circuits controlled separately. This is how it was transformed to do so:

First, the ten 0.5 mm ( $1/50$  in.) diameter shield injection holes (Fig. 1) were filled, thus making the cutter pressure regulator only feed air to the circuit (1). Second, a modified shield cap displayed in Fig. 2B and C was used. It allowed the injection of shield air from a separate source: an independent pressure regulator connected to the pressurized air network.

The shield air is originally injected axially (along X as seen in Fig. 1) through ten shield injection holes. In this paper’s case, shield air is fed radially (Y) through two 4mm ( $1/8$  in.)  $\emptyset$  holes. Thus, one concern about this prototype setup was that the airflow mechanics might have been different from the original design. To lift this doubt, comparative kerfs measurements were performed. Three kerfs were cut with the original setup and then, three other kerfs were cut with the prototype setup. The pressure was set as explained in the

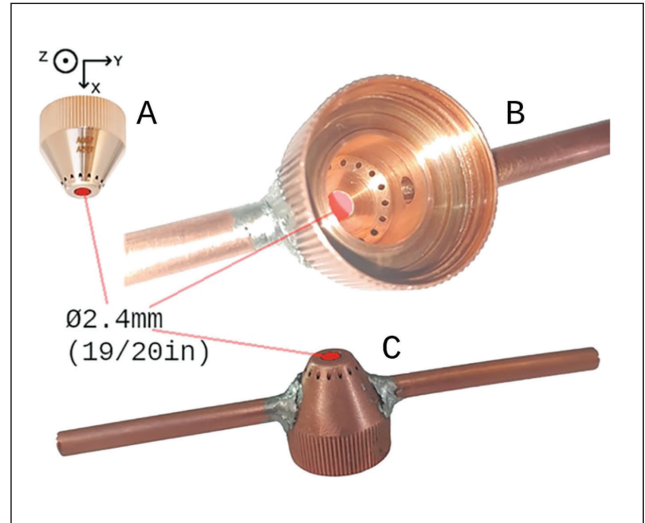


*Fig. 2 – Original (and axes reference): A – Prototype; B-C – shield caps photographs.*

following section to ensure flow rate compliance in both cases. Then the measurements made on these kerfs were compared, leading to similar results in both cases.

### Design of Experiments

The aim was to replicate normal operating conditions flow levels according to the specifications, i.e., when 5 bar (73 psi) is supplied by the cutter pressure regulator to the original torch. In both the original and prototype configuration, let “ $P_1$ ” be the pressure set on the cutter. Only in the prototype setup, let “ $P_2$ ” be the pressure that is fed to the prototype shield cap lateral inlets.  $Q_1$  is the mass flow rate in the swirling air circuit, whereas  $Q_2$  is that of the shield air circuit (Fig. 1). Simultaneous pressure and flow rate measurements were performed. Then two flow rate values above and below these references were chosen to establish the studied pressure domain. This led to the settings presented in Table 1. The flow rate unit used in this paper is NL/min which is normal liter per minute, normal referring to the pressure (1.013 bar / 14.69 psi) and temperature ( $0^\circ\text{C}$  /  $32^\circ\text{F}$ ) of the gas. The flow rates were measured with a SMC PF2A751-04-67 sensor.

Most authors (Refs. 7–11) describe current as a predominant parameter regarding cut quality. Therefore, current was also taken as a varying factor in this study. Increasing the arc current decreases the cutting air flow rate at constant  $P_1$  because plasma is viscous. Consequently, the higher the current (and thus the plasma radius), the higher flow loss it induces. In this paper, the pressures are set but not the airflow rates. The shield gas flow rate is roughly unaffected by the arc current (it only gains 2 NL/min when the arc is shut down from 105 A).

With  $P_1$ ,  $P_2$  and I, a full 3-factor 3-level plan (Table 2) was followed. It led to the 27 sets of parameters. This is the terminology used in this paper regarding the experiments:

A set of parameters is a combination of  $P_1$ ,  $P_2$  and I.

A run consists of the cutting of a kerf/sample at a given set of parameters. There is a total of  $27 \times 3 = 81$  runs.



Fig. 3 – Samples after they were saw-cut: the numbers are those of the sets of parameters; the red circle is where Figure 4 was shot.

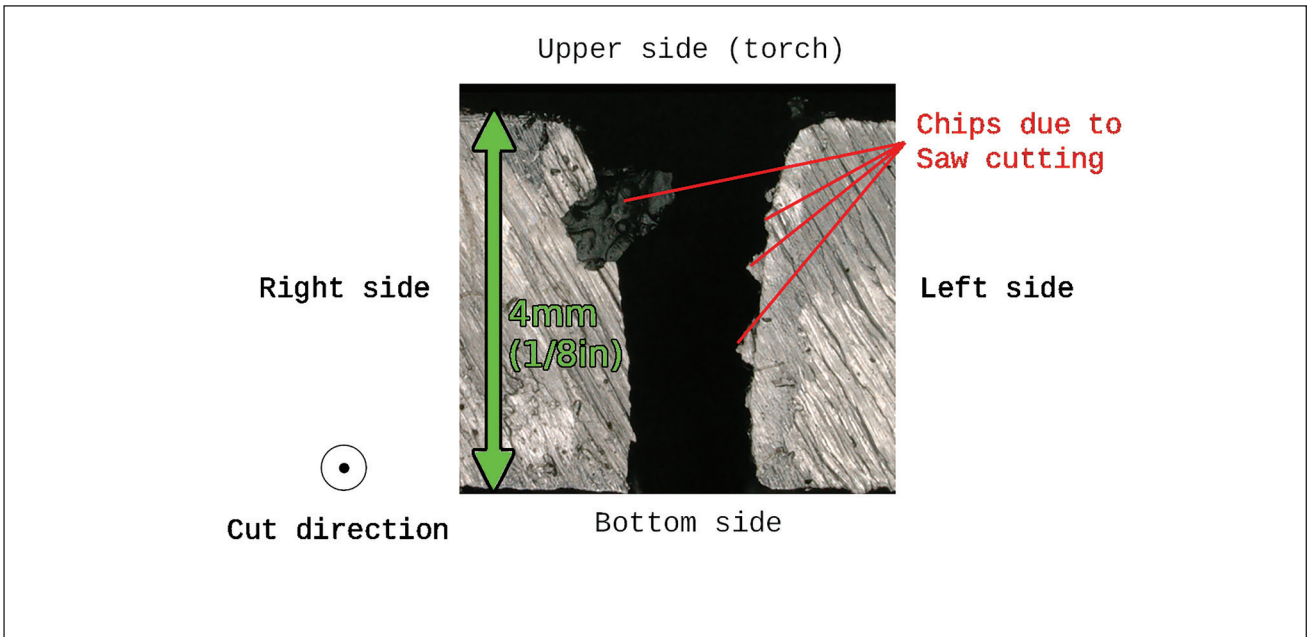


Fig. 4 – Microscope (zoom  $\times 30$ ) view from the sample 25, line 3, with a row of three steel chips and a big chip on the other side due to the saw cutting.

For each set of parameters, one batch of three runs was conducted, so there are 27 batches. The data used in Taguchi's analysis are the averages over the runs within each batch.

The studied responses are described in the next section.

## Cutting Procedure

The plasma cuts were performed on a 4 mm ( $\frac{1}{8}$  in.) thick S355 steel plate. The plate was placed on an *AUTO.TEC* Uni-cut plasma cutting table which also allows the torch to

be moved along three axes. The cuts are made on a single 750 x 500 x 4mm (2.5 ft x 1.6 ft x  $\frac{1}{8}$  in.) S355 steel plate.

Besides the varying factors seen in Table 2, here are the constant cut parameters:

Arc voltage = 160 V (arc voltage is regulated through torch height control)

Cutting speed = 1000 mm/min (3.3 ft/min).

The torch was equipped with fresh consumable parts at the start of the experiment and was used for every 81 runs. The kerfs are 60 mm (2.4 in.) long. This is a sufficiently low workload for the consumable parts not to have any impact

**Table 3 – Overview of the Responses**

	RSS (mm <sup>2</sup> )	LBA (°)	RBA (°)
Overall maximum	15.0	13.0	20.8
Overall minimum	5.9	-3.4	7.4
Overall average	9.5	6.2	12.6

**Table 4 – Effects of the Factors and Effects of the Factors' Interaction**

$E_1 = \text{Effects of } P_1$	$E_2 = \text{Effects of } P_2$	$E_3 = \text{Effects of } I$
$E_4 = \text{Effects of } P_1 - P_2 \text{ (interaction)}$	$E_5 = \text{Effects of } P_1 - I$	$E_6 = \text{Effects of } P_2 - I$

on the results. Figure 3 shows the kerfs layout. Each kerf is separated from the other kerfs in the same batch by a 6 mm gap and each batch is separated from the next in the same column by a 12 mm gap.

It should be noted that Salotinis and Vatousianos (Ref. 9), whose cutting parameters were of the same order of magnitude, measured a HAZ of 0.5 mm (1/8 in.). Therefore, the 6 mm (1/4 in.) separation between each sample is sufficient to avoid cutting inside other kerf's HAZ. Thus, there was no delay between each cut, and the plate was not allowed to cool down. The total time between each cut is due to the torch displacement and represents around 3s. After the plasma cuts, mechanical cuts were performed using a Promac SX-823DG metal band saw. These secondary cuttings were made perpendicular to the thermal kerfs and roughly at midlength to avoid performing measurements within the torch acceleration zones (10 mm 3/8 in.) from each end.

These secondary cutting operations aimed to give access to direct optic measurement by placing the microscope objective in the axis of the kerf. A final task to be performed before making measurements on the samples was to clean them: First, the cutting oil and dross had to be removed, before the kerfs got cleared of the small chips that can appear after a saw cut as seen in Fig. 4. It should be noticed that, in Fig. 4, the right and left sides are given according to the cutting direction, this is why they are flipped around with regards to the page layout.

The following section describes how information was gathered on the samples.

## Measurements Protocol

After preparing the samples, measurements were done using a Keyence VHX-6000 microscope with an X30 zoom.

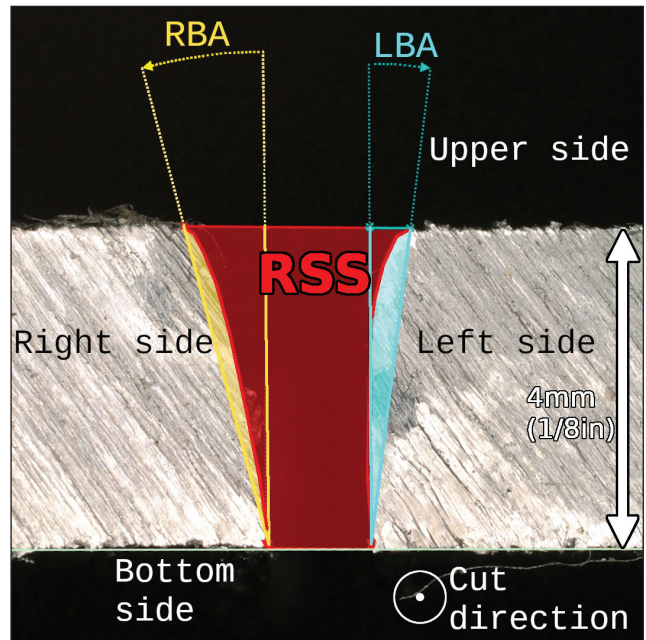


Fig. 5 – Microscope view of a kerf and measurements pattern.

The objective focused on the surface of the plate to obtain the most accurate image. Three quantities were then measured using the built-in measurement tools of the microscope, as shown in Fig. 5.

RSS is the removed steel surface (mm<sup>2</sup>) (1mm<sup>2</sup>=0.0016 in<sup>2</sup>) RBA is the Right bevel angle (°) (right and left being defined with regards to cut direction). A null bevel angle means a vertical kerf. LBA is the Left bevel angle (°).

These three measurements are used as responses in the Taguchi design of experiments. These measurements were made by placing the points manually on the Keyence tool. The way to process these measurements is the subject of the subsequent discussion.

## Results

To conduct this study, Taguchi's method (Ref. 14) was used. This statistical method consists of studying one or several responses to runs conducted at varying factors. It can highlight the effect of each factor independently and their synergistic effects (interaction). The studied factors are the cutting pressure  $P_1$ , the shield air pressure  $P_2$ , and the arc current  $I$ . The studied responses are the removed steel surface RSS and the left and right bevel angles LBA and RBA. An overview of the overall results, encompassing all 81 runs, is presented in Table 3.

## Calculations of the Effects of Each Other and Their Interactions

The effects of the factors and their interactions on a response can be calculated and plotted according to Equations 1 and 2 from Taguchi's methods. These equations are

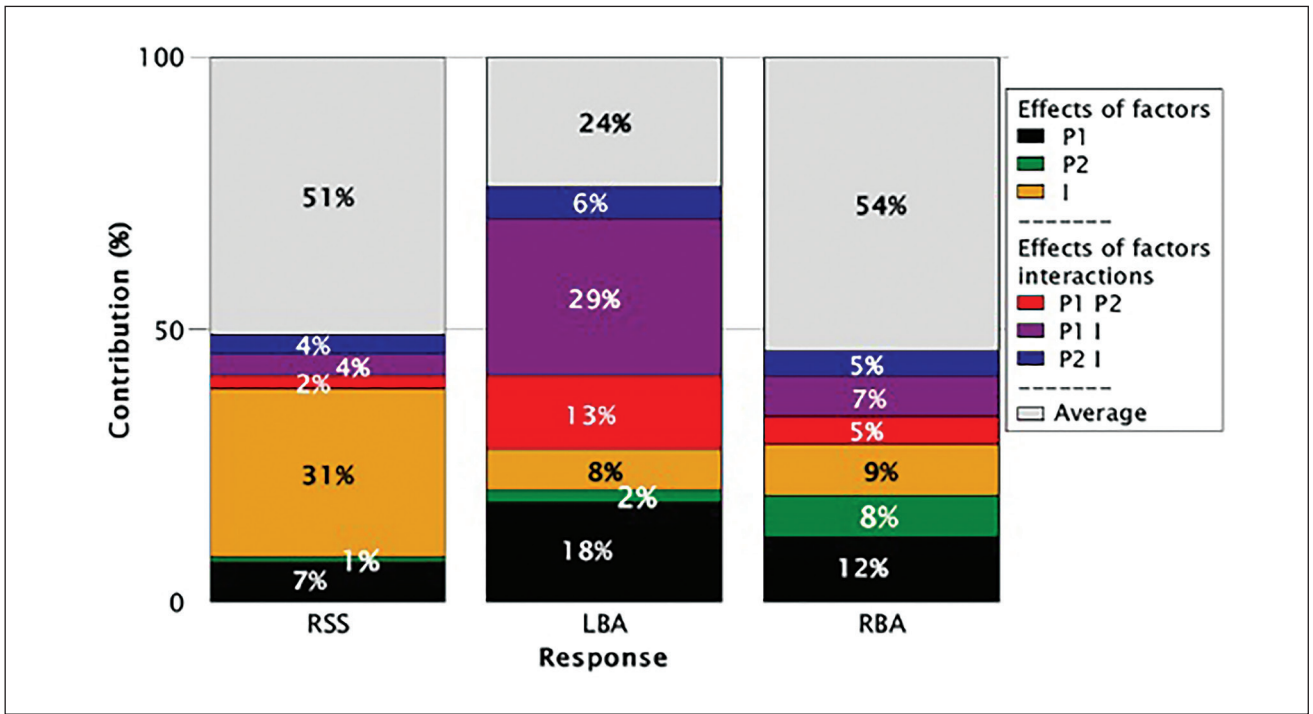


Fig. 6 – Column chart result of a Taguchi-based method showing the contribution of each factor and their interactions.

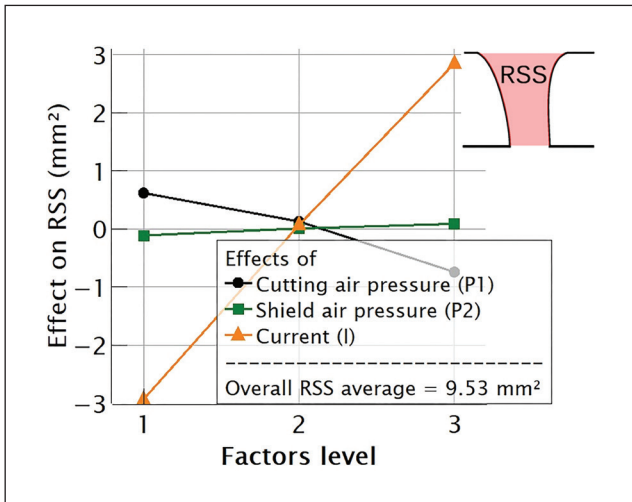


Fig. 7 – Effects on RSS calculated with the Taguchi-based method.

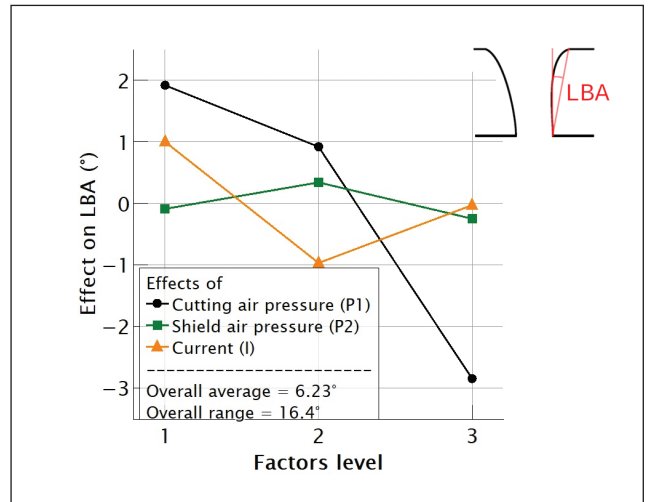


Fig. 8 – Effects on LBA calculated with the Taguchi-based method.

applied to each response independently. It is worth noting that the overall averages are calculated over all 81 runs.

### Effect of Factor A at Level i ( $E_{Ai}$ )

$$E_{Ai} = \text{Average of responses when A is at lvl } i - \text{Overall average} \quad (1)$$

### Effect of the Interaction of Factors A at Level i with B at Level j ( $Int_{Aij}$ )

$$Int_{Aij} = \text{Average of responses when } (A=i \text{ and } B=j) - \text{Overall average} - E_{Ai} - E_{Bj} \quad (2)$$

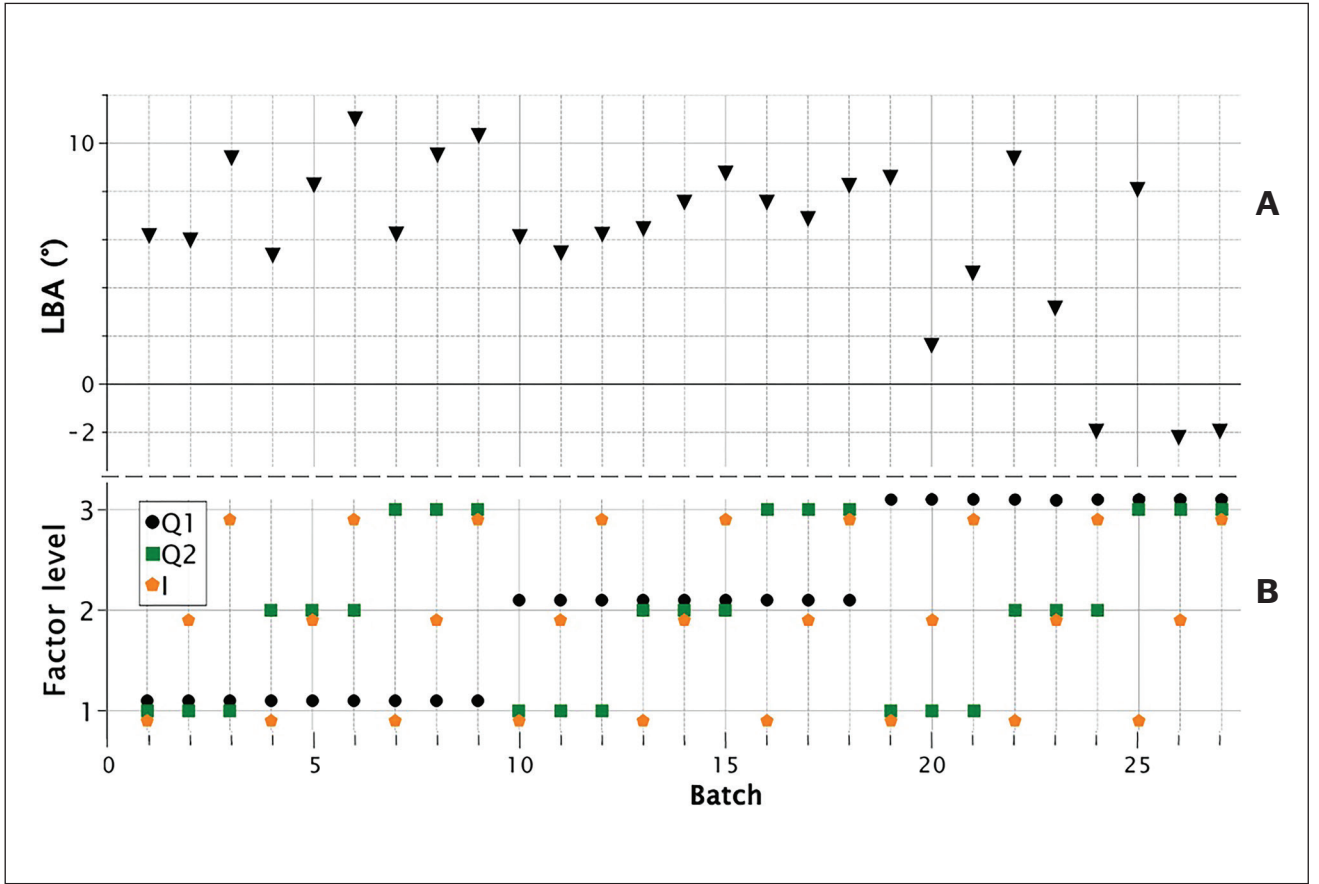


Fig. 9 – A – Left bevel angle values over the experiment; B – corresponding factors levels.

In that case, there are 6 possible effects, 3 from each factor and 3 from their interactions (Table 4).

Let  $n \in N$  and  $1 \leq n \leq 6$ .

Here, the magnitude of the effects was calculated using Equation 3.

### Magnitude of Effect $E_m$ (Mag $E_m$ )

$$MagE_m = MAX(E_m) - MIN(E_m) \quad (3)$$

Next, the contribution of each of the 6 effects (3 from the factors and 3 from their interactions) and of the average on the responses was calculated using Equation 4.

### Contribution of Effect $E_m$ ( $C_{E_m}$ )

$$C_{E_m} = \frac{E_m}{\sum_{n=1}^6 E_n + Overall \ average} \quad (4)$$

Finally, the contribution of the overall average was calculated in the same way using Equation 5.

### Contribution of Effect Overall Average ( $C_{Overall \ avg}$ )

$$C_{Overall \ avg} = \frac{Overall \ average}{\sum_{n=1}^6 E_n + Overall \ average} \quad (5)$$

The contributions calculated through Equations 4 and 5 are plotted in Fig. 6. This shows how each factor (or factor's interaction) affects the response, regarding its average. As a reminder, the factors in this study are  $P_1$  (cutting air pressure),  $P_2$  (shield air pressure), and I (arc current).

A response where the contribution of the factors and their interactions tends towards 0% (and the average towards 100%), would mean that these factors do not impact the responses. For example, it can be seen in Fig. 6 that LBA is the most influenced response (by the studied factors and their interactions) and its average has the smallest contribution. Conversely, RBA is the least influenced response, while RSS is mostly affected by the arc current. Nonetheless, RBA shows a significant influence due to the sole factor  $P_2$  (shield

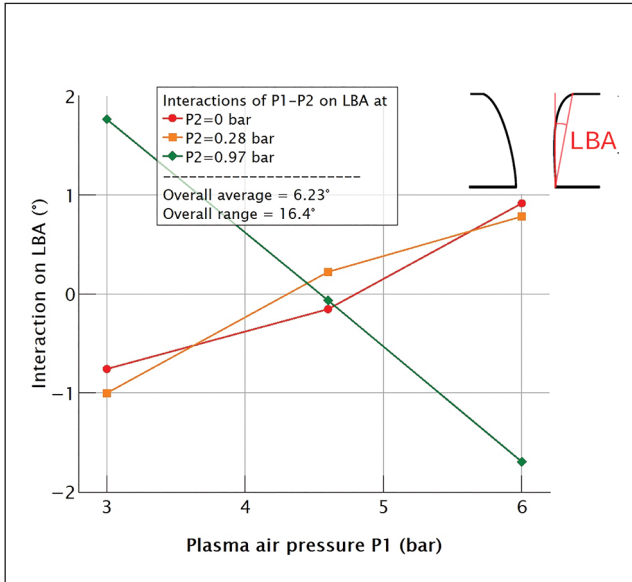


Fig. 10 –  $P_1$ - $P_2$  interactions on LBA calculated with the Taguchi-based method.

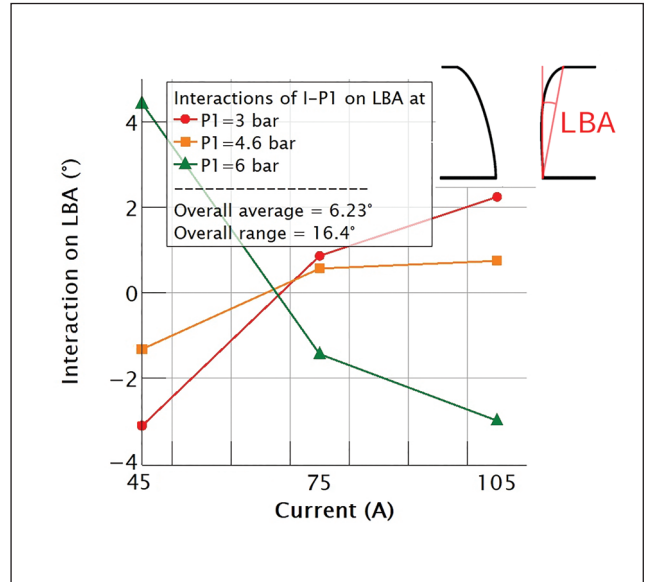


Fig. 11 –  $P_1$ -current interactions on LBA.

air pressure). This study focuses on the effects of shield air pressure, specifically on LBA. The sole factor  $P_2$  has a weak effect, but its interactions with  $P_1$  and  $I$  are important and contribute up to 18% of the LBA response. This will be the subject of deeper discussions, but the two upcoming sections briefly deal with RBA (and why not much attention is given to it) and RSS.

### RBA, the Less Studied Side

Plasma arc cutting kerfs always bring a more vertical side, depending on the cut direction. In this study, every kerf was cut along the same direction and, therefore, RBA is the bigger bevel angle. In an industrial context, this side of the kerf would have little interest and be discarded because most applications need the straightest possible side. As a result, the effects of RBA are not discussed much further in this paper.

### Effects on Removed Steel Surface

As other authors claim (Refs. 9–10), the current proved to be the most impactful parameter to RSS.

Figure 7 represents the effects of each factor on RSS calculated with Equation 1. This is how to read Figs. 7, 8, 10, and 11: The abscissa axis corresponds to the factors level (see Table 2) whereas the ordinate axis represents the effects on the response (RSS in this case). Here is how to read the current curve: at factor level 1, the effect is around  $-3 \text{ mm}^2$  ( $-0.0047 \text{ in.}^2$ ). It means that runs performed at current level 1 (45A) show kerfs smaller than the overall average by  $3 \text{ mm}^2$ . On the other hand, any factors at level 2 involve almost no effect in comparison with the overall experience because these effects are close to  $0 \text{ mm}^2$ .

Increasing the current leads to a significant increase in the kerf width. It is because higher currents lead to wider and

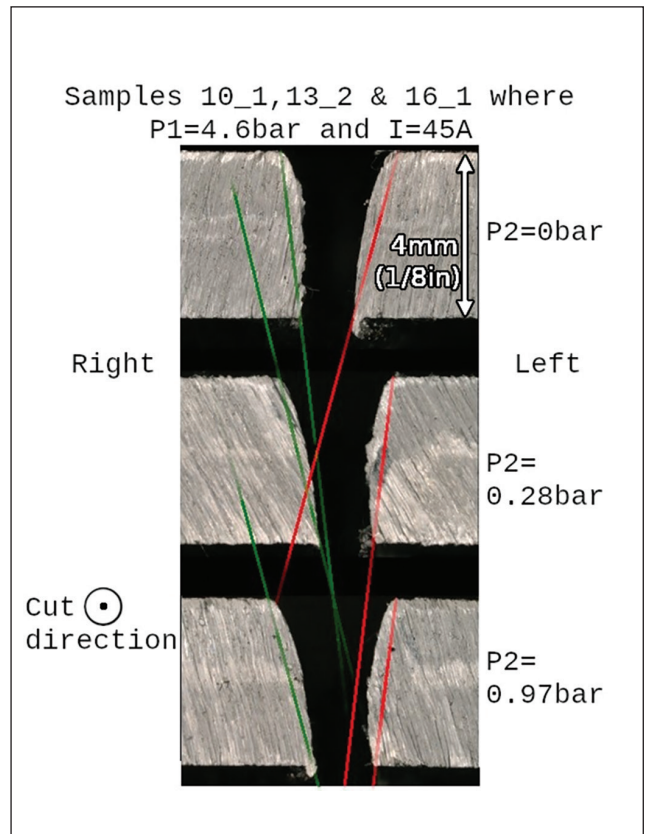


Fig. 12 – Kerf comparison on several microscope views, showing  $P_2$  influence on LBA (red lines) and RBA (green lines).

hotter arcs, melting more metal down. Increasing  $P_1$  has the opposite effect, but a much less strong effect. The right amount of pressure (according to the arc current) is required to remove the molten metal efficiently. In this case, it could be reduced

slightly if the aim was to optimize the material removal rate.  $P_2$ 's influence on RSS is negligible (as seen in Fig. 6).

## Effects on Left Bevel Angle

The bevel angle is a major quality criterion. It must be as close to 0 as possible. As mentioned in the section RBA, the less studied side, only the LBA is given importance in this paper.

With regards to the factors' effects (Fig. 8 calculated with Equation 1), increasing the cutting air pressure is the most significant way to reduce LBA. This may be because increasing the cutting air flow rate leads to faster ejection of the molten steel, thus reducing asymmetry due to molten steel thickness between the top and the bottom of the plate (Ref. 4).

It is important to remember that most bevel angles are positive. The only negative bevel angles occur on LBA in batches 24, 26, and 27 (Fig. 9). Except for these three batches, a negative effect on the bevel angle means a more vertical side. Batches 24, 26 and 27 factors levels [ $P_1$ ,  $P_2$ ,  $I$ ] are respectively [3 2 3] [3 3 2] and [3 3 3]. It appears that all three factors must be high in intensity to bestow enough LBA reduction to turn it negative. However, according to Fig. 8, an isolated high  $P_2$  or  $I$  bring only a very small decrease in LBA (green and orange lines). This indicates that this is  $P_2$  interactions with the other factors allow a greater LBA reduction (as seen in Fig. 10). This is the subject of the two upcoming sections.

### $P_1$ - $P_2$ Interaction on Left Bevel Angle

Taguchi's method allows not only to determine the effects of isolated factors but also that of their interactions. The  $P_1$ - $P_2$  interaction effects on LBA with Fig. 10, whose results calculated with Equation 2 are now detailed.

As expected from the discussion in the preceding section, there is a  $P_1$ - $P_2$  interaction that strengthens the LBA reduction of high  $P_2$  (Fig. 8) when  $P_1$  is also high. At high  $P_1$ , increasing the shield air pressure  $P_2$  leads to an even lower LBA, i.e., to a more vertical side. This is shown by the green line in Fig. 10. It is interesting to note that this tendency is opposite (but weaker) at lower  $P_2$  pressures. A possible explanation would be that, at lower  $P_1$ , the central shield air (Fig. 1) which is fed not axially hinders the axial flow of the cutting air. At higher  $P_1$ , the cutting air might have enough momentum not to be disrupted by the shield air and to pump axially into the kerf, thus contributing more efficiently to molten metal removal.

Consequently, shield pressure should be increased along with cutting pressure to attain better verticality. However, at intermediate cutting pressure, lowering the shield pressure might be considered because it does not hinder verticality. This could be relevant if a strong protection effect is not mandatory (apart from the piercing phase) and if the shield gas must be spared (in the case of a multi-gas system using an expensive shield gas).

### $I$ - $P_1$ Interaction on LBA

Figure 11 shows that, just as with the  $P_1$ - $P_2$  interaction, having high plasma pressure ( $P_1$ ) allows the current's incre-

ment to reduce the left bevel angle, while the opposite effect is seen for lower  $P_1$  values. It means that the current should be increased along with  $P_1$  to attain better verticality (this is not commonly mentioned in the cutters or torch user guides). This is another manifestation of the importance of Current-Pressure balance in plasma arc cutting as discussed in the section Effects on Removed Steel Surface.

Figure 12 shows an example of the shield air pressure  $P_2$  effect at low current and medium plasma air pressure  $P_1$ . The difference between these three samples is the shield air pressure. The red and (resp.) green lines help visualize LBA and (resp.) RBA. The fact they are not parallel shows the influence of  $P_2$  over these angles. In this case, having  $P_2$  go from 0 to 0.28 bar decreases LBA and increases RBA. The difference between 0.28 and 0.97 bar is less sensitive.

## Conclusion

In this paper, the effects of both the cutting and shield air pressures were studied independently. As current is a major criterion when it comes to kerf shaping, it was also considered.

A 3-level 3-factor full plan spanning over current, cutting air, and shield air pressures was followed. A prototype had to be made to allow setting the cutting and shielding pressures separately. However, it was verified that this prototype led to results like those obtained with the base torch (with standard current and airflow rates).

The Taguchi method was used to interpret the results. Kerfs were cut through a steel plate with various sets of parameters and then their dimensions were measured with a microscope. Results were averaged to smoothen scattering. This study concerns the removed steel surface, the right bevel angle, and mostly the left bevel angle.

Naturally, the removed steel surface is largely increasing with higher current values. The air pressure proved less important to this response.

Regarding the bevel angle, a major quality criterion, each of the studied parameters affects it, either directly or through an interaction with another parameter. To attain the straightest left sides (the retained sides, right sides being discarded), a combination of high levels of all three parameters is required. The synergistic effects are interesting because the  $P_1$ - $P_2$  (resp.  $P_1$ -current) interaction effect tendencies get inverted between levels 1 and 2 of  $P_2$  (resp.  $P_1$ ) and level 3.

As a result, to attain better verticality, shield and cutting pressures shall be increased together. This is usually done in existing cutting systems and this study confirms that it is beneficial. In case of low cutting pressures, if the protection from the shield gas does not need to be high and the gas must be spared (if the results are extrapolated to a multi-gas cutter), the shield gas pressure can be reduced even further without affecting verticality.

Also, increasing the cutting pressure along with the current may help get straighter kerfs.

The effect of the shield air pressure  $P_2$  is undeniable because it is required to attain the few negative left bevel angles observed in this study. Indeed, it requires all three factors (including shield air pressure) at high levels to sub-

tract enough bevel angle value, so it turns negative. However, strong  $P_2$  fed at low  $P_1$  leads to skewer kerfs. To conclude, the shield air pressure, apart from its importance in shielding the torch, also has effects on kerf verticality. In existing cutters where it is set along with the cutting pressure, good results can be expected. Finer settings could involve the shield air pressure when possible.

## Acknowledgments

Funding, experimental setups, and technical support provided by SAS Gys.

## References

1. Harničárová, M., Valíček, J., Zajac, J., Hloch, S., Čep, R., Džubáková, I., Tofil, S., Hlaváček, P., Klich, J., and Čepová, L. 2012. *Techno-economical comparison of cutting material by laser, plasma and oxygen*, Teh. Vjesn. 19 813–7.
2. Írsel, G., and Güzey, B. N. 2021. Comparison of laser beam, oxygen and plasma arc cutting methods in terms of their advantages and disadvantages in cutting structural steels. *J. Phys. Conf. Ser.* 2130 012022. DOI: 10.1088/1742-6596/2130/1/012022
3. Hendricks, B. R. 1999. Simulation of plasma arc cutting, submitted towards the degree of master of technology in mechanical engineering. *Cape Peninsula University of Technology*.
4. Nemchinsky, V. A., and Severance, W. S. 2009. Plasma arc cutting speed and cut quality. *J. Phys. D: Appl. Phys.* 42: 195204. DOI: 10.1088/0022-3727/42/19/195204
5. Nemchinsky, V. A. 1996. Liquid metal movement during plasma-arc cutting. *Welding Journal* 75(12): 388-s to 392-s.
6. Gonzalez-Aguilar, J., Sanjurjo, C. P., Rodriguez-Yunta, A., and Calderon, M. A. G. 1999. A theoretical study of a cutting air plasma torch. *IEEE Transactions on Plasma Science* 27(1): 264–271. DOI: 10.1109/27.763132
7. Maity, K. P., and Bagal, D. K. 2015. Effect of process parameters on cut quality of stainless steel of plasma arc cutting using hybrid approach. *The International Journal of Advanced Manufacturing Technology* 78(1–4): 161–175. DOI: 10.1007/s00170-014-6552-6
8. Abdulnaser, B., and Bhuvanesh, R. 2016. Plasma arc cutting optimization parameters for aluminum alloy with two thickness by using taguchi method. *AIP Conf. Proc.* 060002. DOI: 10.1063/1.4958776
9. Salonitis, K., and Vatousianos, S. 2012. Experimental investigation of the plasma arc cutting process. *45<sup>th</sup> CIRP Conference on Manufacturing Systems*, Procedia CIRP 3: 287–292. DOI: 10.1016/j.procir.2012.07.050
10. Ramakrishnan, H., Balasundaram, R., Ganesh N., and Karthikeyan, N. 2018. Experimental investigation of cut quality characteristics on SS321 using plasma arc cutting. *J. Braz. Soc. Mech. Sci. Eng.* 40: 60. DOI: 10.1007/s40430-018-0997-8
11. Ilii, S. M., Coteata, M., and Munteanu, A. 2010. Experimental results concerning the variation of surface roughness parameter (Ra) at plasma arc cutting of a stainless steel workpiece. *International Journal of Modern Manufacturing Technologies* 2(1): 31–36.
12. Nemchinsky, V. A., and Severance, W.-S. 2006. What we know and what we do not know about plasma arc cutting. *J. Phys. D: Appl. Phys.* 39: 423–438. DOI: 10.1088/0022-3727/39/22/R01
13. Colombo, V., Cantoro, G., Ghedini, E., Dallavalle, S., and Vancini, M. 2009. 3D Numerical simulation of a manual plasma cutting torch. *Proceedings ISPC 19*. Bochum.
14. Pillet, M. 2011. Design of experiments using the Taguchi method. ISBN - 978-2-9539428-0-4

**SEBASTIEN CHABERT** ([chabert@laplace.univ-tlse.fr](mailto:chabert@laplace.univ-tlse.fr)), **JEAN-JACQUES GONZALEZ**, and **PIERRE FRETON** are with the Laboratoire Plasma et Conversion d’Energie, Université de Toulouse, Toulouse, France. **CHABERT** is also with SAS GYS, Saint-Berthevin, France.